PAPER • OPEN ACCESS

CFD investigation of flatback airfoils and swallow tail for wind turbine blades

To cite this article: C Solombrino et al 2024 J. Phys.: Conf. Ser. 2767 022017

View the article online for updates and enhancements.

You may also like

- Optimal design of aeroacoustic airfoils with owl-inspired trailing-edge serrations
 Mingzhi Zhao, Huijing Cao, Mingming Zhang et al.
- Development of a morphing flap using shape memory alloy actuators: the aerodynamic characteristics of a morphing flap Seung-Hee Ko, Jae-Sung Bae and Jin-Ho Rho
- Experimental study of a passive control of airfoil lift using bioinspired feather flap Longjun Wang, Md Mahbub Alam and Yu Zhou.



doi:10.1088/1742-6596/2767/2/022017

CFD investigation of flatback airfoils and swallow tail for wind turbine blades

C Solombrino 1,2 , A Koodly Ravishankara 1 , H Özdemir 2 , and C H Venner 2

- 1 TNO, Wind Energy, Energy and Materials Transition, Westerduinweg 3, 1755 LE Petten, NL 2
- ² Engineering Fluid Dynamics, Department of Thermal and Fluid Engineering, University of Twente

E-mail: akshay.koodlyravishankara@tno.nl

Abstract. Modern wind turbines use longer blades to improve annual energy production. Longer blades require thicker airfoils for structural integrity. Thicker airfoils are susceptible to issues like erosion, abrupt stalls, and early boundary layer transition, leading to increased drag and decreased lift, affecting overall performance. Flatback airfoils offer structural and aerodynamic advantages, being stiffer, less sensitive to surface roughness. However, this comes with a drag penalty, mainly due to the increase in base drag. Swallow tail add-on has been proposed to overcome these challenges. URANS simulations are used to analyze the aerodynamic performance of the different airfoils and hybrid RANS/LES simulations are used to study the flow features in more detail. The swallow tail airfoil was found to maintain many of the advantages of the flatback airfoils while reducing the drag penalty.

1. Introduction

In order to increase the annual energy production, modern wind turbine blades are longer, sweeping a larger area to capture more wind and generate more power. However, this also increases the overall blade and rotor weight and causes an increase in gravitational and aerodynamic loads on the blades and the support structures. Heavier structures use more material driving up the cost of wind energy. Therefore, design choices for wind turbine blades that can generate the same power while keeping them slender are needed. Structural stiffness in the blades could be gained by adopting thick airfoils in the inboard region of the blade. However, thick airfoils are generally prone to premature transition from laminar flow due to surface contamination [1] and abrupt stall.

To improve the poor aerodynamic performance of thick airfoils, flatback airfoils (FB) have been introduced. These are created by symmetrically adding thickness to the aft half of the airfoil (figure 1). The increased thickness at the trailing edge reduces the curvature of the suction side and alleviates the adverse pressure gradient and premature flow separation resulting in a higher maximum lift and larger lift slope [2]. However, this comes with a drag penalty, mainly due to the increase in base drag. The low pressure near the trailing edge causes vortex shedding, typical of bluff-body wake, which results in high drag values. This drag penalty can be reduced by means of trailing edge add-ons [3, 4, 5]. In particular, an add-on called "swallow tail" (figure 1) [6, 7] has been shown to reduce the unsteadiness of the wake thereby the drag.

Content from this work may be used under the terms of the Creative Commons Attribution 4.0 licence. Any further distribution of this work must maintain attribution to the author(s) and the title of the work, journal citation and DOI.

doi:10.1088/1742-6596/2767/2/022017

The objective of the present work is to numerically investigate the aerodynamics of flatback and swallow tail airfoils using RANS (Reynolds Averaged Navier Stokes) and hybrid RANS/LES (Large Eddy Simulations) simulations. New swallow tail designs based on the patent application [6] are proposed and the capability of these designs to overcome the drawbacks of the flatback airfoil is investigated. The following simulations are performed:

- 2D RANS and URANS (Unsteady RANS) for the regular airfoil and 2D URANS for the flatback and swallow tail airfoils.
- 3D hybrid RANS/LES for the flatback and the swallow tail geometries.

A schematic view of the airfoils involved in this study is shown in figure 1. The DU97-W-300 airfoil is used as the basis for the design of the flatback and the swallow tail airfoils.

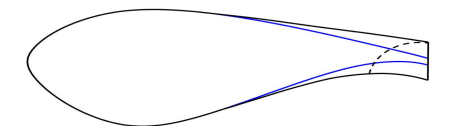


Figure 1: Schematic geometries of the airfoils considered in this study based on the DU97-W-300: regular (blue), flatback (black), swallow tail (dashed).

The paper is organised as follows - the design of the swallow tail concept is explained in section 2. Section 3 presents the numerical setup used for the analysis. Section 4 shows the 2D results from the URANS simulations. In section 5, hybrid RANS/LES results are used to closely examine the features responsible for the drag penalty of the flatback airfoil and to show how the swallow tail design overcomes these limitations. Finally, section 6 contains the conclusions from this study.

2. Swallow Tail design

The purpose of the swallow tail design is to reduce the drag of the flatback airfoil while maintaining its advantages. The general indications given in the patent application [6] for the design of a swallow tail from a flatback airfoil are to cut off the pressure side curve (at $\approx 10\%c$) in order to create a non-symmetrical cavity. These features suppress the coupling between the vortices generated from the pressure and suction sides. Furthermore, to have a more realistic design a finite trailing edge thickness equal to that of the regular airfoil is chosen. The design parameters considered in developing the swallow tail geometry used in the present study, shown in figure 2, are:

- (i) Trailing edge thickness, t_{TE}
- (ii) Length of pressure side cut-off, L.
- (iii) The curvature of arc between the above two points measured by the concavity angle, β

The curvature of the arc must be chosen to be sufficiently large to create a non-symmetrical cavity and at the same time limit its concavity to ensure that the flow from the lower side separates towards the upper one and does not recirculate within the cavity. The DU97-W-300-FB airfoil is chosen as the basis for the swallow tail design. Two different designs, denoted by ST1 and ST2, were considered.

3. Numerical set up

3.1. SU2

The open source software SU2 is used for the numerical simulations [8, 9, 10]. The governing equations have the following structure [9]

$$\partial_t U + \nabla \cdot F^C - \nabla \cdot F^V = Q,\tag{1}$$

doi:10.1088/1742-6596/2767/2/022017



Figure 2: Swallow tail design parameters: trailing edge thickness t_{TE} , length of pressure side cut-off L and concavity angle β . The values of these parameters for the two designs ST1 and ST2 are also given.

where U represents the vector of state variables, $F^C(U)$ and $F^V(U)$ are the convective and viscous fluxes and Q(U) the source term. The second order Jameson-Schmidt-Turkel (JST) scheme is used to discretize the convective fluxes. Spatial gradients are computed using Green-Gauss and weighted least-squares methods for the 2D and 3D simulations respectively [10]. Time integration is carried out with a second order dual time stepping approach [11] in combination with the implicit Euler scheme [10]. Finally, the turbulence closure equations are solved with a first order scalar upwind method.

3.2. Turbulence modeling

2D RANS and URANS simulations have been performed using the SST turbulence model. For the 3D simulations a non-zonal hybrid RANS/LES approach called Enhanced Delayed Detached Eddy Simulation (EDDES) [12, 13] based on the Detached Eddy Simulation (DES) [14] is used, which models the boundary layers with RANS and resolves separated regions and wakes with LES. The underlying sub grid scale (SGS) model is based on the one equation SA [15] turbulence model. The sub grid length scale for the LES formulation is the Shear Layer Adapted (SLA) length scale whose argument is a grid-independent definition of a parameter called the Vortex Tilting Measure (VTM). This is a kinematic measure that identifies the quasi 2D areas in the initial shear layers where the turbulence instabilities have to be developed. VTM is close to zero in quasi 2D flow regions and varies in a range of values near one in regions of developed 3D turbulence [13]. All simulation cases are fully turbulent.

3.3. Mesh and Boundary Conditions

A chord length of c=1m is used for all cases. Three grids with 128, 258, and 516 nodes around the airfoil surface have been tested. The airfoils are meshed with an O-grid topology, with the far field boundary located approximately 100c from the airfoil. The initial cell height is set to achieve a $y+\approx 1$ for an appropriate resolution of the viscous sublayer. The growth rate of the cell height is 1.1 for the 2D URANS cases. For the 3D cases, a growth rate of 1.05 is used for the near airfoil region and 1.08 in the rest of the domain. In the spanwise direction a constant spacing of $\Delta y=0.05c$ is used.

A no-slip boundary condition on the airfoil is used. On the circular domain the far-field boundary condition is applied. Periodic boundary conditions are applied in the spanwise direction, which extends to 2c.

4. 2D Results

In sections 4.1 and 4.2 the results from the grid and time refinement studies are shown. In section 4.3, results from the preliminary analysis of the two swallow tail designs are given. Based on these results, lift and drag coefficient polars for the different airfoil designs are presented in section 4.4.

doi:10.1088/1742-6596/2767/2/022017

4.1. Grid refinement results

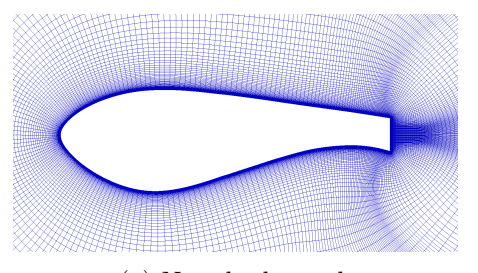
The flow around the regular DU97-W-300 airfoil at an angle of attack of $\alpha = 4^{\circ}$ at $Re = 1.6 \times 10^{6}$ is investigated. The lift and drag coefficients, C_l and C_d are given in table 1. Here N refers to the number of grid points on the airfoil surface. The C_l is almost identical for all three grids but a change in C_d is observed between N = 128 and N = 258 grids. Based on these results, the N = 258 grid was selected for the successive investigations. The results from this grid closely match the results from RFOIL [16], a widely used airfoil analysis tool based on XFOIL [17].

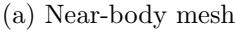
Grid (N)	$\alpha [\mathrm{deg}]$	C_l	C_d
128	4	0.71	0.0199
258	4	0.70	0.0185
516	4	0.70	0.0183
RFOIL	4	0.74	0.0184

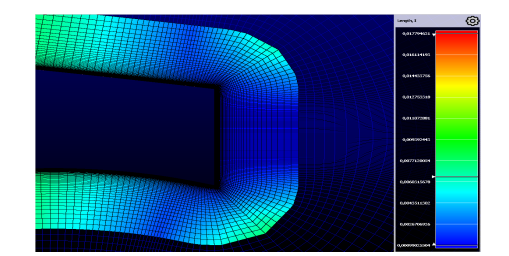
Table 1: 2D RANS grid refinement study on the regular DU97-W-300 airfoil, $Re = 1.6 \times 10^6$. N denotes the number of points along the airfoil. RFOIL values given as an independent reference.

4.2. Time step refinement results

2D URANS simulations of the flatback version of the DU97-W-300 airfoil (DU97-W-300-FB) at two different angles of attack, $\alpha = 4.4^{\circ}, 11.6^{\circ}$ at $Re = 1.6 \times 10^{6}$ are performed. Based on the grid refinement study given in 4.1, the grid with N = 258 nodes around the airfoil surface is used. 100 points on the TE are needed to ensure a smooth match between the cells on the suction and pressure side of the airfoil and the TE (figure 3b).







(b) Chord-wise length of the cells around the TE

Figure 3: Near-body mesh for the DU97-W-300-FB airfoil profile (left) with close-up to the trailing edge (right).

Time step [sec]	$\alpha [\mathrm{deg}]$	C_l	C_d	$\alpha [\mathrm{deg}]$	C_l	C_d
dt = 0.00015	4.4	0.87	0.0718	11.6	1.73	0.0569
dt = 0.0003	4.4	0.87	0.0679	11.6	1.75	0.0594
dt = 0.0006	4.4	0.86	0.0668	11.6	1.75	0.0611
experiments tripped	4.4	0.83	_	11.6	1.74	-

Table 2: Time refinement study using 2D URANS on the DU97-W-300-FB compared to the experimental data [3], $Re = 1.6 \times 10^6$.

The time refinement results are shown in table 2. At low angle of attack ($\alpha = 4.4^{\circ}$), the C_l values are the same for dt = 0.00015 and dt = 0.0003. For the higher angle of attack ($\alpha = 11.6^{\circ}$), the obtained C_l values differ of only 0.01%. Furthermore, the C_l experimental value is an average of the two. Hence, the time step dt = 0.0003 is considered a good compromise between accuracy and computational time. This will be used in the successive 2D URANS simulations.

doi:10.1088/1742-6596/2767/2/022017

4.3. Swallow tail analysis

Aerodynamic investigations are carried out for $Re=1.6\times10^6$ at an angle of attack $\alpha=11.6^\circ$ where the strongest eddies were observed with the flatback airfoil. A first design (ST1) was made based on the guidelines in [6] with a large cut-off from the pressure side and a steep curvature $(L=0.101c,\,\beta=70^\circ)$. The lift and drag coefficients are listed in table 3. It can be seen that the resulting lift coefficient is significantly lower than the flatback, but importantly also lower than the regular airfoil. The efficiency is however higher than both the regular and flatback airfoil. To address the issue of the low lift coefficient, a second design (denoted by ST2) is proposed. The cut-off length was made shorter and the curvature smaller with L=0.049c and $\beta=40^\circ$. This resulted in an increased lift coefficient and an increase in efficiency of 43% compared to the flatback airfoil and 26% compared to the regular airfoil. Importantly, the lift coefficient is now higher than for the regular airfoil.

Airfoil	$\alpha[\deg]$	C_l	C_d	C_l/C_d
Regular	11.9	1.32	0.0397	33.37
Flatback	11.6	1.75	0.0594	29.40
Swallow tail 1 (ST1)	11.6	1.19	0.0288	41.37
Swallow tail 2 (ST2)	11.6	1.42	0.0337	42.09

Table 3: Aerodynamic coefficients and efficiency for the different airfoil designs at $Re = 1.6 \times 10^6$.

Figure 4 shows the instantaneous velocity contours at an angle of attack, $\alpha=11.6^{\circ}$, and Reynolds number, $Re=1.6\times10^{6}$. Flow separation is visible on the suction side of the regular airfoil (figure 4a). Vortex shedding from the trailing edge of the flatback airfoil is seen clearly in figure 4b. However, no flow separation is observed and the flow remains attached. Similarly, no flow separation is observed for both ST1 and ST2 designs (figures 4c and 4d). Additionally, relatively little to no vortex shedding is observed for either of the two designs. Thus, it can be seen that the swallow tail retains the advantages of the flatback while reducing the drawbacks: the separation on the suction side is postponed and the wake unsteadiness is reduced.

4.4. URANS polars

Given the better lift characteristics, the swallow tail ST2 is further analyzed and compared to the flatback and regular airfoils over a range of angles of attack at $Re=3\times 10^6$ where experimental data for both the regular and FB airfoils is available [18, 19]. In the experiments, the flow is tripped at x/c=0.05 on the suction side and at x/c=0.20 on the pressure side for the regular airfoil and x/c=0.05 and x/c=0.10 on the suction and pressure side respectively. The numerical results are not expected to match the experimental data exactly since it is not possible to accurately capture the effect of tripping on the boundary layer development. Additionally, the small laminar region of the flow before the tripping is not simulated. The polars are given in figure 5. The URANS results match closely with the experimental data for both the regular and FB airfoils. However, for the regular airfoil the URANS stall prediction deviates significantly from experiments.

Amongst the three airfoils, the flatback airfoil has the highest $C_{l,max}$. Despite lower lift in the linear region, the swallow tail has a higher $C_{l,max}$ than the regular airfoil. Post stall a constant lift value is observed. The flatback airfoil shows the largest C_d value, which remains quite constant for a broad AoA range. A reduction in drag just before the stall is observed for the FB airfoil which has also been reported in the literature [20]. On the contrary, the regular airfoil presents the lowest drag values but only up to an angle of attack of approximately $\alpha = 9^{\circ}$. The C_d values of the swallow tail are slightly higher than the regular airfoil but substantially lower than the FB airfoil (up to 52%) and also remain constant for a wide range of angles of attack.

doi:10.1088/1742-6596/2767/2/022017

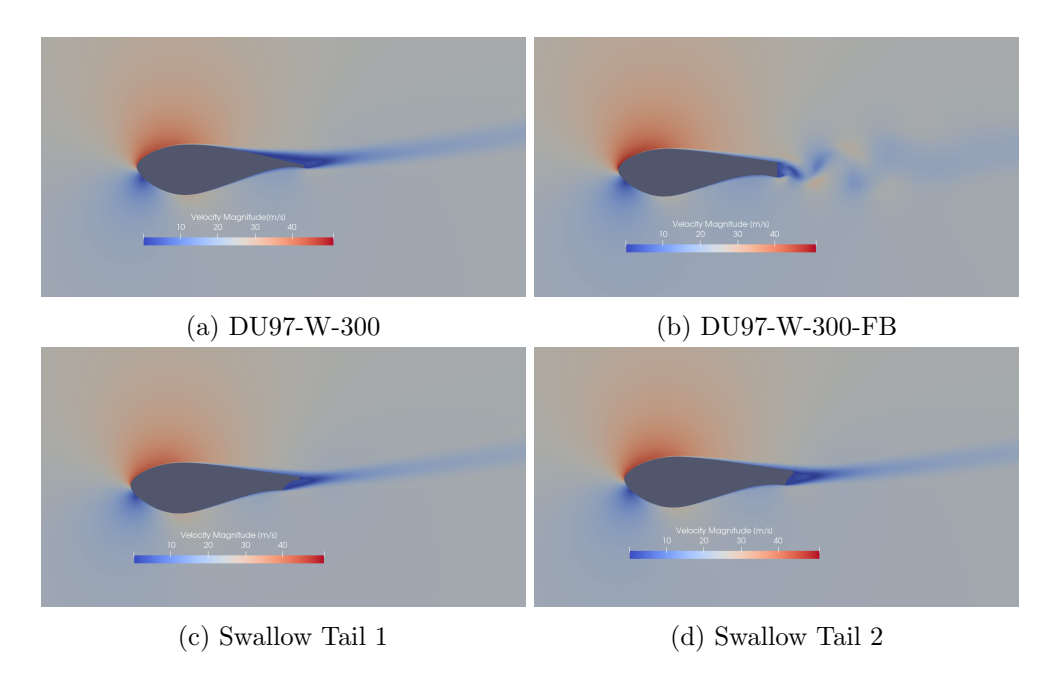


Figure 4: Instantaneous velocity contours from 2D URANS for different airfoils at $Re = 1.6 \times 10^6$, $\alpha = 11.6^{\circ}$. Flow separation is observed for the regular airfoil and vortex shedding for the flatback airfoil. Both swallow tail designs show no separation.

The aerodynamic efficiency is shown in figure 5c. The swallow tail concept outperforms the flatback airfoil for all the angles of attack tested, with an increase in efficiency up to 60% from approximately $\alpha=6^{\circ}$ till stall. At low angles of attack when the flow is attached, the regular airfoil shows higher efficiency while at higher angles of attack, from $\alpha=9^{\circ}$ onwards where the regular airfoil stalls, the swallow tail shows higher efficiency. This behavior is analogous to that observed for airfoils with vortex generators.

5. 3D EDDES Results

To further investigate the relevant flow physics for drag reduction, a higher fidelity analysis of the flatback airfoil and the swallow tail design ST2 is performed. In a companion study [21], the effect of spanwise extent was investigated and a span size of 2c was chosen.

5.1. DU97-W-300FB

In figure 6, the mean pressure coefficients C_p obtained with EDDES and 2D URANS are compared to the experimental results. The mean C_p predictions obtained with EDDES follow the experimental data for both the angles of attack tested. At $\alpha = 4.4^{\circ}$, it can be seen that the mean C_p distribution obtained with 2D URANS overlaps the EDDES one. However, at $\alpha = 11.6^{\circ}$, towards the TE, the URANS result moves away from the experimental data, while the EDDES remains close to it.

The main contribution to the drag in flatback airfoils is due to the base drag, which is caused by a low pressure behind the trailing edge. This can be visualized in figure 7a where a clear low pressure region behind the trailing edge is observed. This leads to vortex formation and shedding from the trailing edge as seen in the figure 7b.

doi:10.1088/1742-6596/2767/2/022017

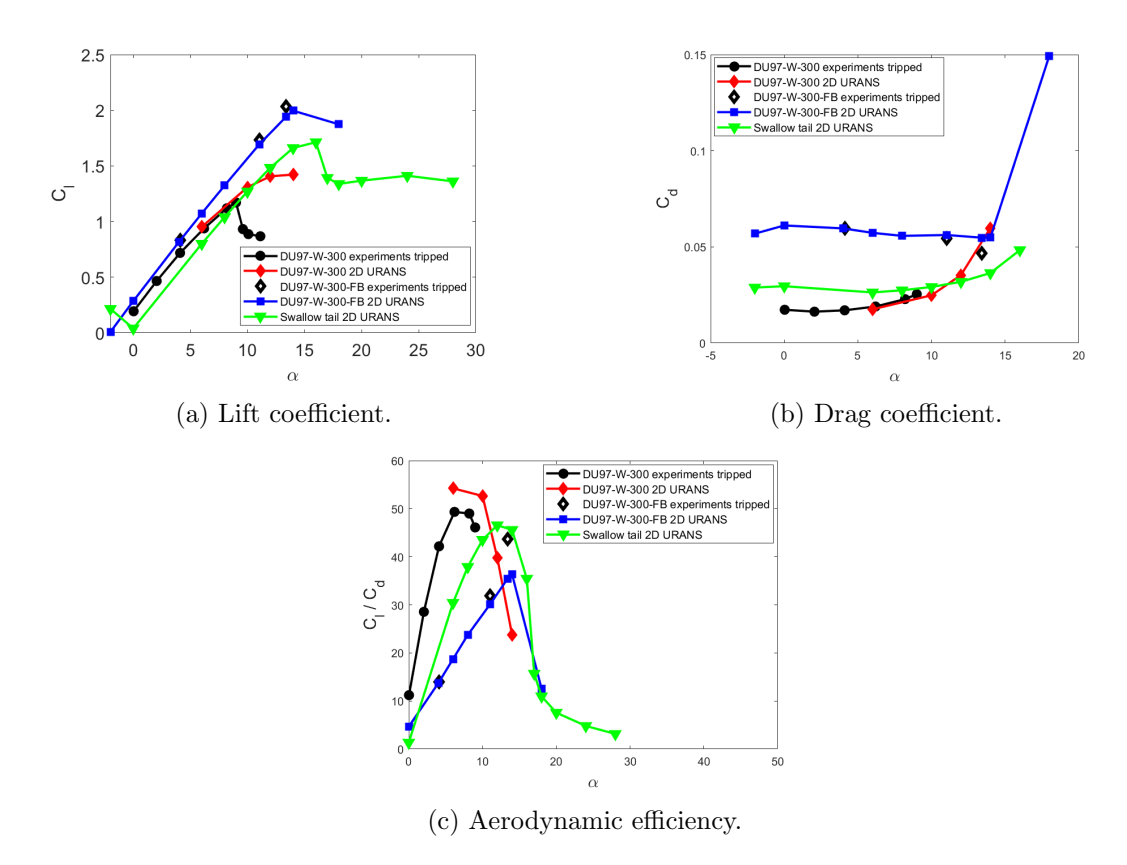


Figure 5: Lift and drag polars for the regular, flatback and swallow tail airfoils at $Re = 3 \times 10^6$

5.2. Swallow tail

A 3D EDDES simulation with spanwise extent 2c is performed for $\alpha=11.6^{\circ}$. The low pressure region behind the trailing edge was identified as the main reason for drag increase in flatback airfoils. Figure 8a shows the mean pressure coefficient along the span and figure 8b compares the pressure level along the span from the swallow tail and the flatback airfoils just behind the trailing edge (x/c=1.05 and z/c=-0.03). A larger pressure region is observed along the trailing edge of the swallow tail which leads to a reduction in the base pressure drag compared to the flatback airfoil. Figure 9 compares the iso-surfaces of the Q criterion (0 < Q < 6000) between the flatback airfoil and the swallow tail airfoil. Regular vortices that span the entire width of the domain can be seen behind the flatback airfoil in figure 9a. However, the vortical structures behind the swallow tail are more irregular and break apart closer to the trailing edge. As expected the absence of the low pressure region behind the trailing edge leads to a reduction in the periodic vortex shedding. Additionally, the flow on the surface of the airfoils is similar for both concepts.

5.3. Strouhal number

The power spectral density (PSD) of the lift fluctuations as a function of Strouhal number $(St = fh_{TE}/U_{\infty})$ using the TE height $(h_{TE} = 0.17c)$ of the flatback airfoil is shown in figure 10. A peak is observed at St = 0.12 for the flatback airfoil and at St = 0.18 for the swallow tail. In figure 10 the amplitude of the PSD is normalized with the peak of the flatback airfoil. It can be seen that for the swallow tail, the shedding occurs at a higher frequency and with a reduced amplitude of about 50% compared to the flatback. The shift of the peak to higher frequency and the reduction in the amplitude of the spectra indicate a reduction in vortex shedding from

doi:10.1088/1742-6596/2767/2/022017

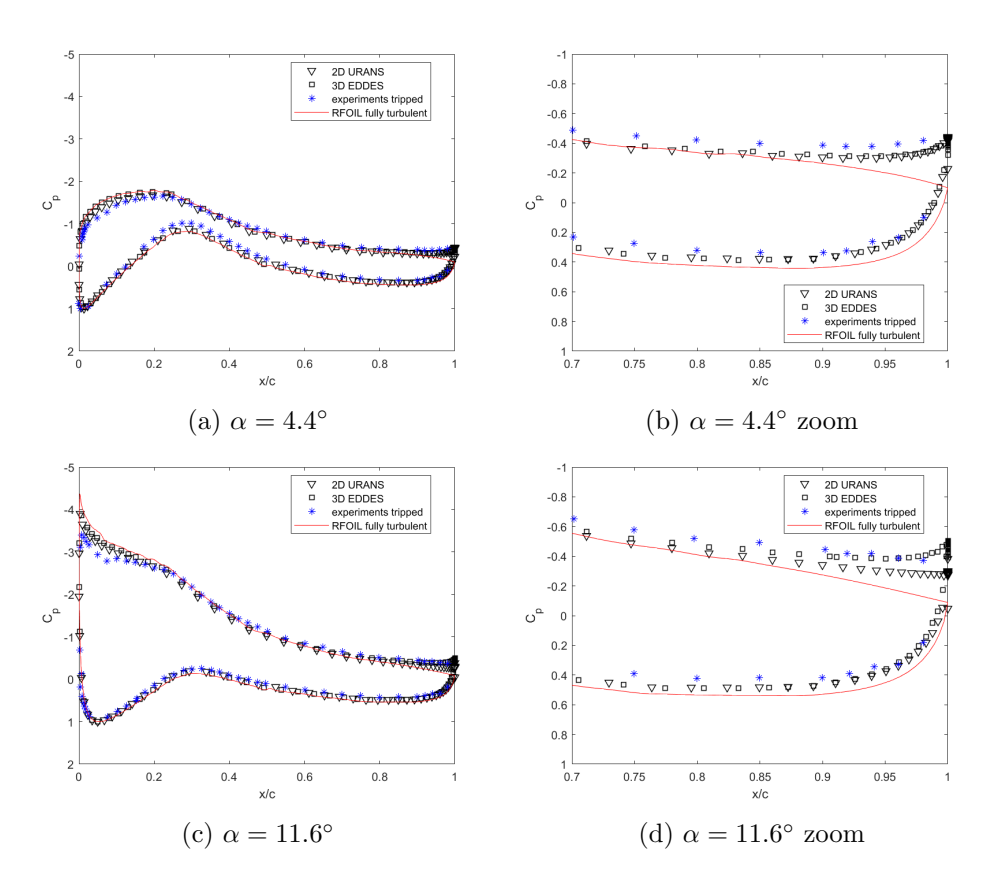


Figure 6: Mean C_p for DU97-W-300-FB from RFOIL, URANS and EDDES at different angles of attack and $Re = 1.6 \times 10^6$. The behavior near the trailing edge is also shown. Only the EDDES matches the experiments at both angles of attack.



(a) Mean C_p contour for the flatback.

(b) Instantaneous normalized velocity streamlines.

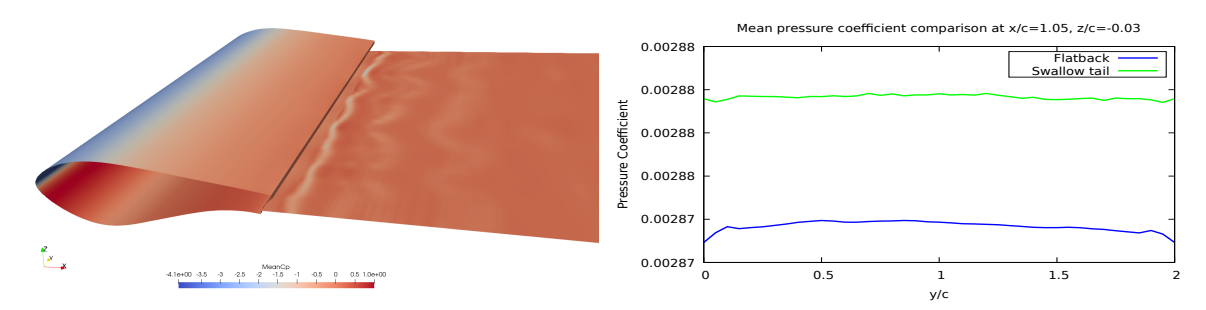
Figure 7: Mean C_p for DU97-W-300-FB and velocity streamline at $Re = 1.6 \times 10^6$, $\alpha = 11.6^\circ$. A low pressure region is observed behind the trailing edge. The resulting vortex roll-up can be seen in the instantaneous velocity streamlines.

the swallow tail compared to the flatback airfoil.

6. Conclusions

The flow around flatback and swallow tail airfoils has been investigated numerically using URANS and EDDES. The advantages of the flatback airfoil i.e. delayed flow separation and a

doi:10.1088/1742-6596/2767/2/022017



- (a) Mean C_p contour for the swallow tail design.
- (b) Base pressure level comparison.

Figure 8: Mean pressure coefficient (C_p) for the swallow tail at $Re = 1.6 \times 10^6$, $\alpha = 11.6^\circ$. On the right, the mean pressure coefficient behind the trailing $\mathrm{edge}(x/c = 1.05, z/c = -0.05)$ of the airfoil is compared between the swallow tail (green) and the flatback airfoil (blue). A much lower pressure level is observed for the flatback airfoil.

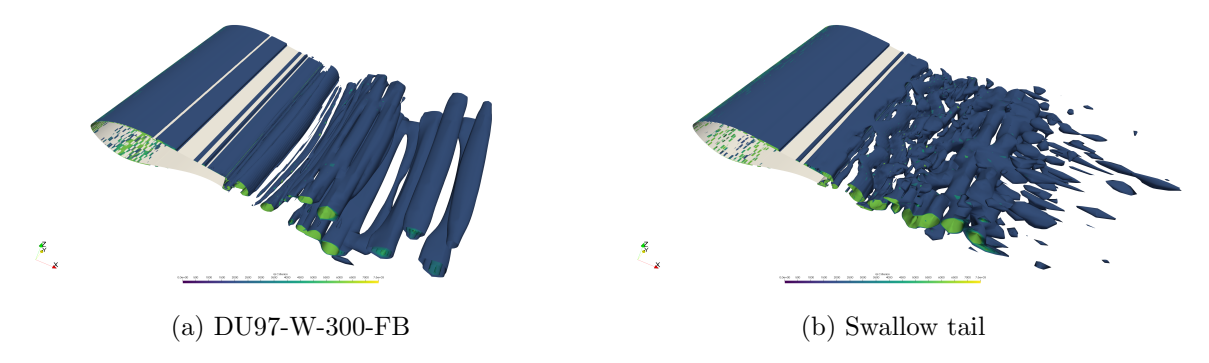


Figure 9: Instantaneous isosurfaces of Q-criterion at $Re = 1.6 \times 10^6$, $\alpha = 11.6^\circ$. Regular vortex structures are visible behind the flatback airfoil unlike the swallow tail, where the vortex structures break down earlier.

higher lift slope compared to the regular airfoil were demonstrated. The presence of the vortex shedding due to the low pressure behind the trailing edge which results in a drag penalty was clearly observed in the high-fidelity simulations.

To overcome the drag penalty of the flatback airfoil, the concept of swallow tail was examined. Two different designs were analyzed. Lift and drag polars were computed over a wide range of angles of attack using 2D URANS. The lift slope of the swallow tail airfoil was lower than that of the regular airfoil in the attached flow region but it had a higher $C_{l,max}$ and a larger stall angle. The drag values for the swallow tail are generally higher than for the regular airfoil but substantially lower than for the flatback airfoil. The swallow tail reduces the drag by up to 52% for low angles of attack resulting in an increase in efficiency up to 60% compared to the flatback airfoil.

Further investigations of the swallow tail with 3D EDDES shows that while vortex shedding is observed with the swallow tail concept as well, it is less severe compared to the flatback airfoil and appears to break apart quicker. The PSD analysis shows that the amplitude of the vortex shedding is reduced by about 50% while increasing its frequency.

In conclusion, the swallow tail airfoil was shown to retain many of the advantages of the flatback airfoil over a regular airfoil while minimizing many of its drawbacks.

doi:10.1088/1742-6596/2767/2/022017

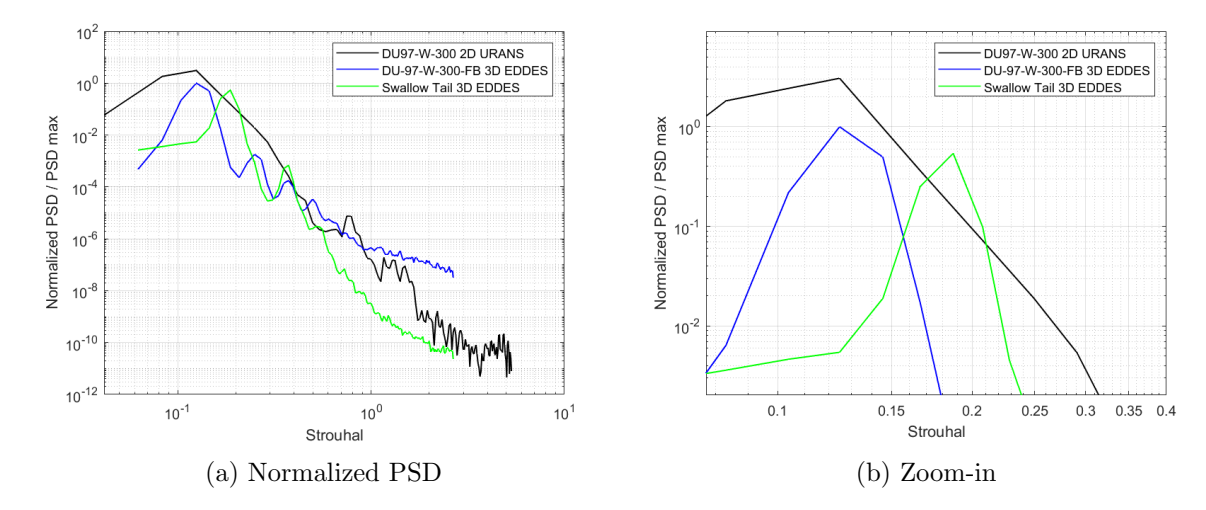


Figure 10: Frequency spectrum based on the C_l time series for the regular, flatback and swallow tail airfoils at $Re = 1.6 \times 10^6$, $\alpha = 11.6^\circ$. A shift towards higher frequencies and a reduction in amplitude for the swallow tail compared to the flatback airfoil can be seen.

References

- Standish K J and Dam C P V 2003 Journal of Solar Energy Engineering, Transactions of the ASME 125(4) 479–487 ISSN 01996231
- [2] Baker J, Mayda E and van Dam C 2006 44th AIAA Aerospace Sciences Meeting and Exhibit p 193
- [3] Barone M F, Berg D E, Devenport W J and Burdisso R 2009 Technical Report No. SAND2009-4185, Sandia National Laboratory
- [4] Baker J, Van Dam C and Gilbert B 2008 SAND Series Albuquerque, N. M. (Sandia National Laboratories)
- [5] Manolesos M and Voutsinas S G 2016 AIAA Journal 54 3382–3396
- [6] Grasso F 2018 United States Patent US0238298A1
- [7] Yilmaz O C and Timmer W A 2018 (American Institute of Aeronautics and Astronautics Inc, AIAA)
- [8] Economon T D, Palacios F, Copeland S R, Lukaczyk T W and Alonso J J 2016 AIAA Journal 54(3) 828–846ISSN 00011452
- [9] Palacios F, Alonso J, Duraisamy K, Colonno M, Hicken J, Aranake A, Campos A, Copeland S, Economon T, Lonkar A, Lukaczyk T and Taylor T 51st AIAA Aerospace Sciences Meeting including the New Horizons Forum and Aerospace Exposition
- [10] Palacios F, Economon T D, Aranake A, Copeland S R, Lonkar A K, Lukaczyk T W, Manosalvas D E, Naik K R, Padron S, Tracey B, Variyar A and Alonso J J 2014 (American Institute of Aeronautics and Astronautics)
- [11] Jameson A and Shankaran S 2009 19th AIAA Computational Fluid Dynamics
- [12] Shur M L, Spalart P R, Strelets M K and Travin A K 2015 Flow, Turbulence and Combustion 95(4) 709–737 ISSN 15731987
- [13] Molina E, Spode C, da Silva R G A, Manosalvas-Kjono D E, Nimmagadda S, Economon T D, Alonso J J and Righi M 2017 23rd AIAA Computational Fluid Dynamics Conference
- [14] Spalart P R, Jou W H, Strelets M K and Allmaras S R 1997 Proceedings of first AFOSR international conference on DNS/LES 1 4–8
- [15] Spalart P R and Allmaras S R 1992 30th Aerospace Sciences Meeting and Exhibit (AIAA) ISSN 00341223
- [16] Van Rooij R 1996 Delft University of Technology
- [17] Drela M 2001 Aeronautics and Astronautics Dept., Massachusetts Inst. of Technology, Cambridge, MA
- [18] Barone M and Berg D 2009 47th AIAA Aerospace Sciences Meeting including The New Horizons Forum and Aerospace Exposition p 271
- [19] Timmer W A and Rooij R P V 2003 Journal of Solar Energy Engineering, Transactions of the ASME 125(4) 488–496 ISSN 01996231
- [20] Manolesos M and Papadakis G 2021 Physics of Fluids 33 085106 ISSN 1070-6631
- [21] Solombrino C 2023 University of Twente URL http://essay.utwente.nl/97815/